Flexible strain sensor enabled by carbon nanotubes-decorated electrospun TPU membrane for human motion monitoring

*Xin Yu [‡a], Zijian Wu [‡*a,b], Ling Weng [*a,b], Dawei Jiang [c], Hassan Algadi [d,e],*

*Zhuofan Qin[f], Zhanhu Guo[*f] and Ben Bin Xu[*f]*

[a]Department of Material Science and Technology, Harbin University of Science and Technology, Harbin 150040, China

[b]Key Laboratory of Engineering Dielectric and Its Application Technology of Ministry of Education, Harbin University of Science and Technology, Harbin 150040, China

[c]Heilongjiang Key Laboratory of Molecular Design and Preparation of Flame Retarded Materials, Northeast Forestry University, Harbin 150040, China

[d] Department of Electrical Engineering, Faculty of Engineering, Najran University, Najran, 11001, Saudi Arabia

[e]College of Materials Science and Engineering, Taiyuan University of Science and Technology, Taiyuan, 030024, China

[f] Mechanical and Construction Engineering, Faculty of Engineering and Environment, Northumbria University, Newcastle Upon Tyne, NE1 8ST, UK

‡ Equal contribution

*Corresponding author.

Email: zijian.wu@hrbust.edu.cn; wengling79@163.com; nanomaterials2000@gmail.com; ben.xu@northumbria.ac.uk

Keywords: Flexible sensor, Electrospun, Dopamine modification, Fitted model

Abstract:

High-performance flexible strain sensors are gaining more and more attention with their bespoken detection range, excellent sensing performance and good stability, which are highly desired in the wearable electronics. Herein, a thermoplastic polyurethane elastomer (TPU) fibrous membrane was prepared as a flexible substrate by electrostatic spinning technology, then a coating of polydopamine was formed through fast synthesizing the dopamine on TPU fibrous membrane surface and loaded with CNTs to develop an extremely sensitive flexible strain sensor. The flexible sensor prepared by TPU fibrous membrane coated with polydopamine layer has an outstanding sensibility under the pulling force (GF of 10528.53 with 200% strain), rapid reaction time (188-221 ms), wide sensing range (up to 200%), good stability and durability. The theoretical studies reveals that the underlying cause for the high sensitivity and the inherit relationship between the amount of conducting routes and the length between adjacent conducting fillers in the sensor. The demonstration of device shows a promising application to sense the human motion at various locations of body, with accurate and stable electrical signal output generated at corresponding motion.

Introduction

With the advent of new era of flexible wearable devices, strain sensors have gradually become a hot spot of attention in academia and industry [1-6]. Strain sensors have a broad range of encouraging utilizations in the areas of human motion monitoring, flexible electronic skin, medical diagnosis, and human-machine interface [7-19]. Conventional sensors are composed of rigid materials, which are hard and brittle in texture and difficult to curl, and cannot meet the applications in some specific fields, which require stretchable conductors that can maintain stable electrical conductivity even when undergoing large deformations. Conductive polymer composites (CPCs) have good flexibility and good tensile properties to meet the environment of sensors under large tensile (strain ≥ 50%) and bending conditions.

Common flexible strain sensors choose flexible polymer materials with good stretchability as substrate layer, including polydimethylsiloxane (PDMS) [20-24], thermoplastic polyurethane elastomer (TPU) [25-27] and Ecoflex [28, 29]. Commonly, flexible strain sensors usually incorporate nanometals (such as metal nanoparticles, silver nanowires) [30-32], nanocarbon materials (including carbon black, CNTs, graphene, etc.) [33-45], conductive polymers (including PANI, PPy, and PEDOT:PSS) [46-49], and other conducting materials like Mxene [50-52] as conductive fillers with polymeric substrates to impart excellent electrical conductivity to the composites.

A broad detection range and a lower monitoring limit are key criteria for a stretchable and flexible strain sensor. A low monitoring limit of sensor allows a fast and accurate response to a small strain stimulus, which is crucial for real-time monitoring of human motions and human health. The wider detection range can satisfy the use of sensor at a larger strain. In recent years, electrostatic spinning has been widely used as a micro/nanofiber preparation technology due to its preparation of electrospinning membrane with big specific surface area, large porosity, good mechanical flexibility, and its simple and efficient preparation method [53-57]. Among them, TPU is simply electrostatically spun into fibrous membranes, that exhibit excellent tensile properties, flexibility, and mechanical strength [58, 59]. As a kind of emerging nanomaterials, CNTs are also

widely used in many fields [60-64]. Selecting suitable materials to prepare various sensors has become the research focus of scholars at home and abroad [65-71]. Li *et al.* [72] prepared a flexible sensor with the wide monitoring range and ultralow detection limit by ultrasonically anchoring CNTs to TPU electrospun membrane. However, it also shows a disadvantage of low sensitivity limit, which is less desirable in a condition requiring high sensitivity. The flexible sensors with high sensitivity, good responsiveness, and a wide detection range remain yet to be developed.

In this work, TPU fibrous membrane was prepared as a flexible substrate by electrostatic spinning, and the TPU fibrous membrane was coated with dopamine (DA) self-polymerization (named DT), and CNTs particles were introduced on the substrate by filtration to build the conductive layer (coded as CT and CDT). We systematically studied the impact of introducing polydopamine layer on conductive layer, the surface morphologies of the CT sensor as well as the CDT sensor, the mechanical properties of the CT and CDT samples and the differences in sensing properties during stretching, and the mechanical hysteresis of this samples with the dependencies on different substrate structures [73-75]. A mathematical model leads the understanding on the variation of resistance with strain ($\Delta R/R_0$) by using tunnelling theory, and is used to analyse the sensitivity between CT and CDT samples caused by the length of neighbouring conductive fillers and the amount of conducting routes was analyzed to provide an explanation by calculating the parameters of this mathematical model. The final prepared CDT sensor has a low detection limit (less than 1%), a broad detecting range (up to 200%), an extremely high sensitivity (GF of 10528.53 at 200% strain), and great cycle stability due to the presence of the polydopamine layer, which can respond accurately to various human movements and even vocalizations.

Result and discussion

1. Preparation of high sensitivity sensor

The preparation of stretchable CNTs/DA/TPU flexible strain sensor is illustrated in Figure 1, the experimental details are described in the *Methods*. We assign a code name of CT for the CNT coated TPU flexible strain sensor, and CDT for CNTs/DA/TPU flexible strain sensor.

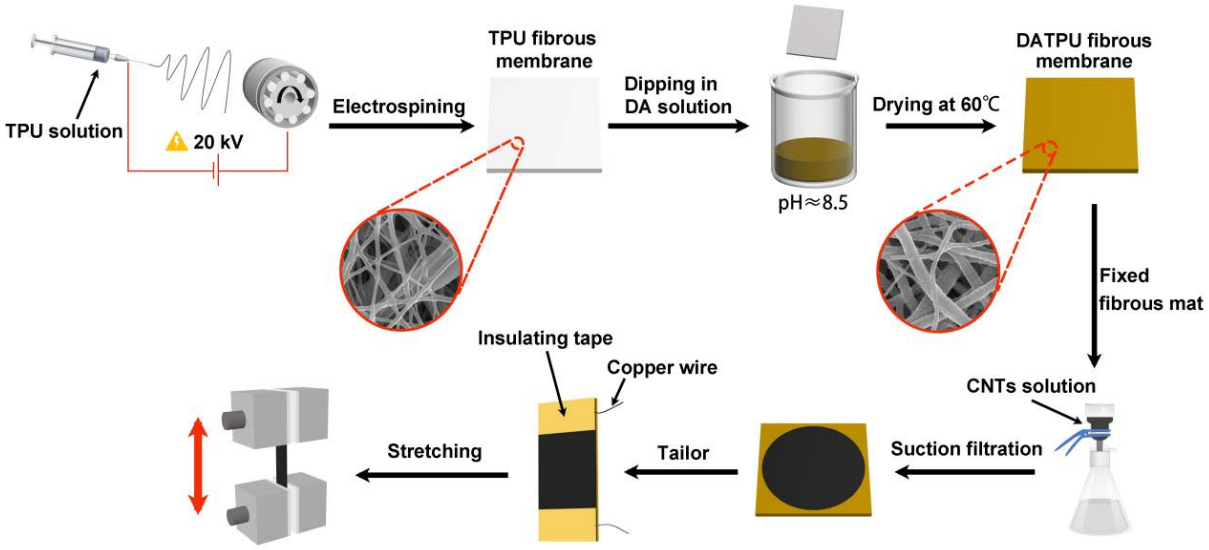

Figure.1 Schematic diagram of the preparation of CNTs/DA/TPU flexible strain sensor.

The morphology of the prepared conductive fibrous membranes is revealed in Figure. 2. The surface of pure TPU fibers appear to be relatively even (Figure. 2 a,b), a small amount of CNTs was loaded on the surface of TPU fibers after binding with CNTs (Figure. 2 e,f). The surface of DATPU prepared after dopamine coating was rougher (Figure. 2 c,d), and was completely coated by CNTs after binding with CNTs (Figure. 2 g,h). This may be caused by that DA underwent self-polymerization on the TPU surface to form a polydopamine layer and uniformly coated the TPU fibers, which increased the roughness of the fiber surface and was able to bind more CNTs to the fibers surface when pumping the same content of CNTs suspension.

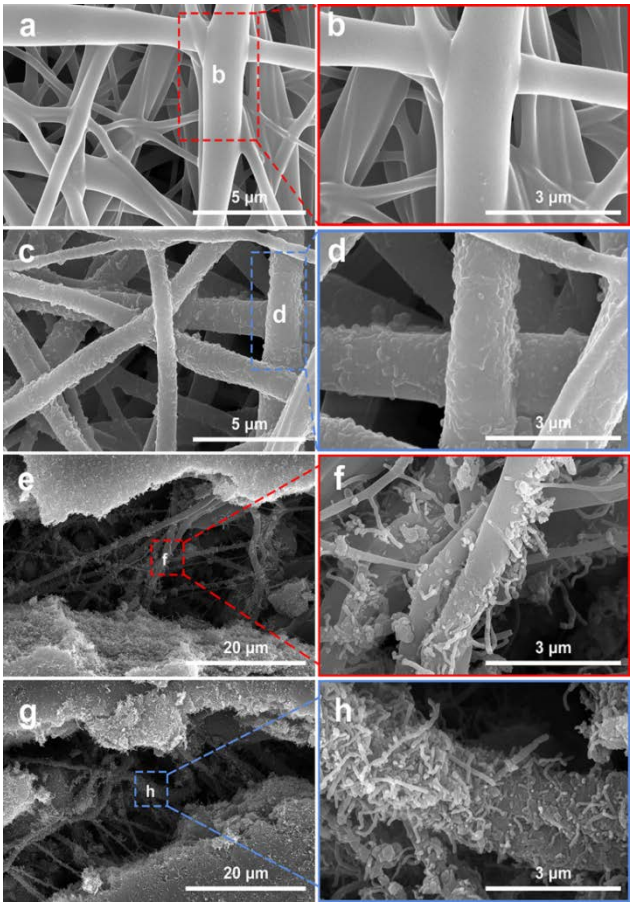

Figure. 2 a-b TPU electrospun membrane, c-d DA/TPU fibrous membrane, e-f CNTs/TPU flexible strain sensor, g-h Scanning electron microscope images of CNTs/DA/TPU flexible strain sensor.

The loading of carbon nanotubes plays a critical role in determining the conductivity of fibrous membrane. CNTs suspensions of (2.5 ml/5 ml/7.5 ml/10 ml/15 ml) with a concentration of 2g/L were pumped onto TPU electrospun membranes to control the loading of CNTs. The relative resistance of CNTs/TPU flexible strain sensors with different CNTs loadings at 10~50% strain is shown in Figure. 3a. The relative resistance of CNTs/TPU flexible sensors showed an increasing trend at 10% and 30% strain with increasing CNTs loadings, but the maximum relative resistance of flexible strain sensors with 15 ml of CNTs suspension pumped at 50% strain was about 38.39. However, the maximum relative resistance of flexible sensor with 15 ml of CNTs suspension at 50% strain was about 38.39, while the maximum relative

resistance of flexible sensor with 10 ml of CNTs suspension is about 59.62, indicating a significant decrease in the relative resistance.

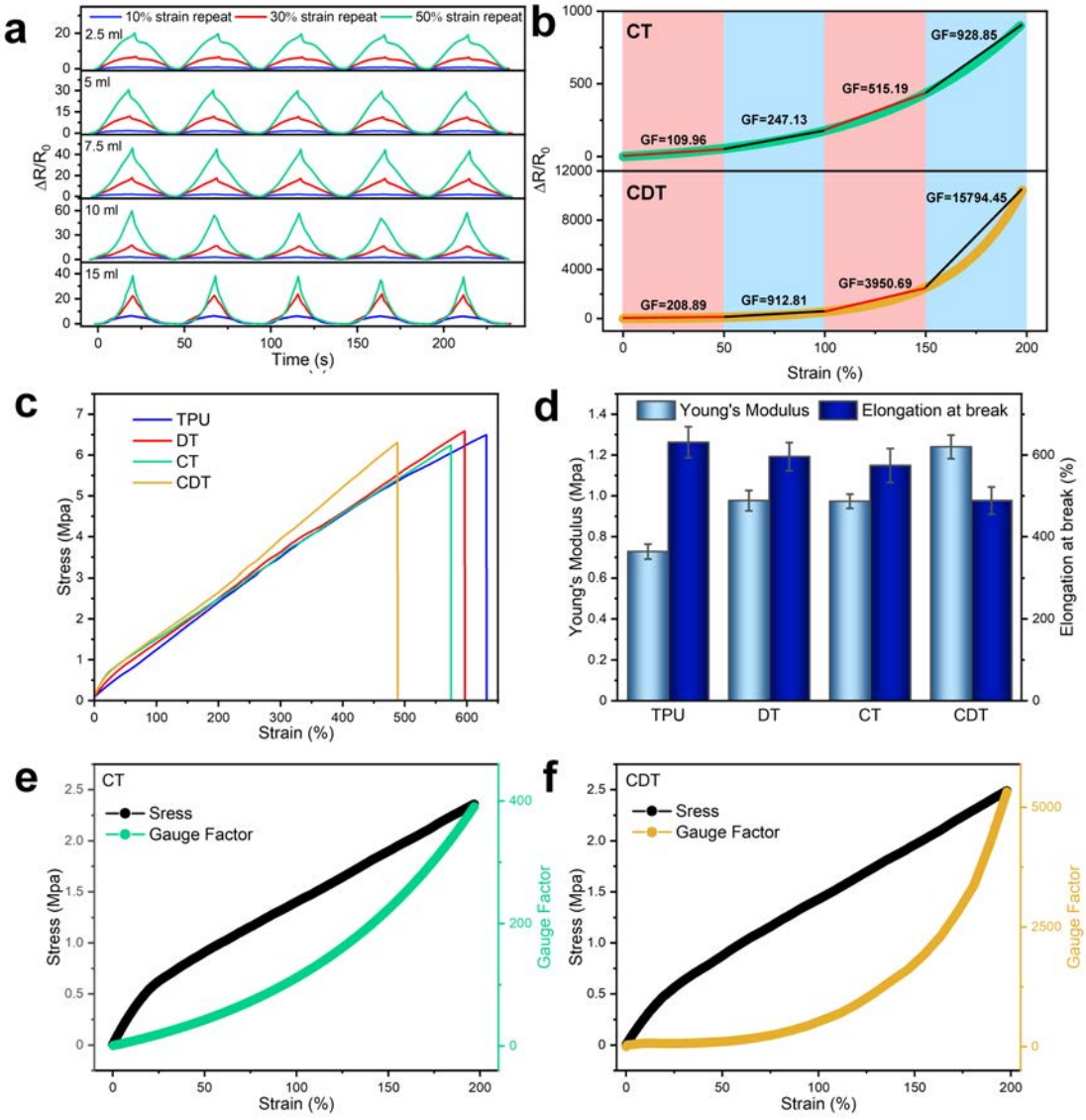

Figure. 3 The relative resistance of CNTs/TPU flexible strain sensors at 10%, 30%, and 50% strain at CNTs draws from 2.5 ml to 15 ml, b Sensitivity of CT sensors and CDT sensors in four regions from 0-200% strain, c Typical stress-strain curves, d Young's modulus of TPU, DT, CT, and CDT samples and fracture Elongation, e-f Sensitivity of CT and CDT sensors at 0-200% tensile range per unit strain (GF).

The hypothetic reason is that the specimen underwent the process of destruction and reconstruction of conducting network with cyclic stretching, the conductive pathway constructed on the TPU substrate gradually increased as the load of CNTs increased, and the

destruction of the conductive pathway increased at the same strain. However, when the loading of CNTs continues to increase to certain amount, most conductive pathways are still not completely destroyed under larger strains, and the conductive networks of conductive fillers are still lapped, causing a significant decrease in relative resistance. A flexible strain sensor with a 10ml suspension of CNTs was considered to be an optimal set for application.

2. Mechanical properties and sensing performance of CT and CDT flexible strain sensors

We further studied the strain sensing performance and mechanism of high gauge factor in the CT and CDT sensors. In general, the GF (Gauge Factor) is a crucial parameter to assess the sensing performance, identified as the ratio of relative resistance change to strain, and can be calculated by equation (1):

$$GF = (\Delta R/R_0)/\varepsilon, \varepsilon = \Delta L/L_0 \quad (1)$$

where the R_0 and ε are the initial resistance and applied strain, respectively. ΔR is the difference between the real-time resistance and the initial resistance.

Figure 3b compares the sensitivity of CT and CDT flexible strain sensors in four regions from 0-200% strain, where the GF values of CT flexible strain sensor are 109.96 (0-50% strain), 247.13 (50-100% strain), 515.19 (100-150% strain), and 928.85 (150-200% strain), respectively. The GF values of CDT flexible strain sensors were 208.89 (0-50% strain), 912.81 (50-100% strain), 3950.69 (100-150% strain), and 15794.45 (150-200% strain). It can be observed that the gauge factors of CDT sensor are higher than those of the CT sensor in all strain regions, empowered by the polydopamine layer wrapped fiber surface. Figure 3c shows the typical stress-strain curves of conductive composite fibrous membrane, the tensile strength of prepared pure TPU fibrous membrane is 6.49 ± 0.12 Mpa, and the tensile strength of DATPU fibrous membrane is 6.58 ± 0.11 Mpa, the tensile strength of the dopamine-coated TPU fibrous membrane is increased by about 0.1 Mpa. In addition, the tensile strength of prepared CT sensor is 6.24±0.21 Mpa for the CT sensor and 6.31±0.15 Mpa for the CDT sensor, It can be observed

that the tensile strength of TPU fibrous membrane increased after being coated with dopamine, which interacts more strongly with it.

In addition, the Young's modulus of pure TPU fibrous membrane in Figure 3d reached 0.73 Mpa and the elongation at break was 631% ± 37%. the Young's modulus of DATPU fiber membrane reached 0.98 Mpa and the elongation at break was 596% ± 34%. With the introduction of dopamine, the Young's modulus of fibrous membranes increased significantly, however, the elongation at break decreased, probably due to the strong bonding ability between the PDA coating and TPU fibers and the strong inter- and intramolecular hydrogen bonding exhibited by both the PDA coating and the PDA and TPU matrix [76]. Also compared to CT (Young's modulus 0.97 Mpa, elongation at break 574% ± 33%), the Young's modulus of CDT was more significantly improved by 0.27 Mpa with a Yang's modulus of 1.24 Mpa, nevertheless, its elongation also decreased significantly with a CDT elongation at break of 488% ± 30%, which could be attributed to the polydopamine layer and more CNTs attached between the fibers, which helps to reduce the slip between fibers [77]. To further compare the sensitivity of CT sensor with that of the CDT sensor, the GFs of both sensors were compared at 0-200% strain, corresponding to 399.66 and 5322.82 for CT and CDT, respectively, further illustrating the better responsiveness of CDT (Figure 3 e,f).

3. Mechanical Hysteresis of strain sensor

The long-term stability as well as the durability of sensors are important for applications in detecting real time motion. Figure 4a,b shows the cyclic loading and unloading curves for 20 cycles at 10% strain for the CT and CDT sensors, respectively, with the red line showing the first cycle and the blue line showing cycles 2-20. Mechanical hysteresis (H_M) is an effective indicator to guide the construction of internal conductive network of CT and CDT sensors, as we need minimize H_M when the sensors undergo multiple loading and unloading cycles [73, 74].

From Figure 4c, the (A_L-A_U) area and the A_U area are represented in orange and green, respectively. The H_M value could be measured from equation (2) as follows.

$$H_M = \frac{|A_L - A_U|}{A_L} \quad (2)$$

Where A_L is the integral area of the loading curve to the x-axis and A_U is the integral area of the unloading curve to the x-axis.

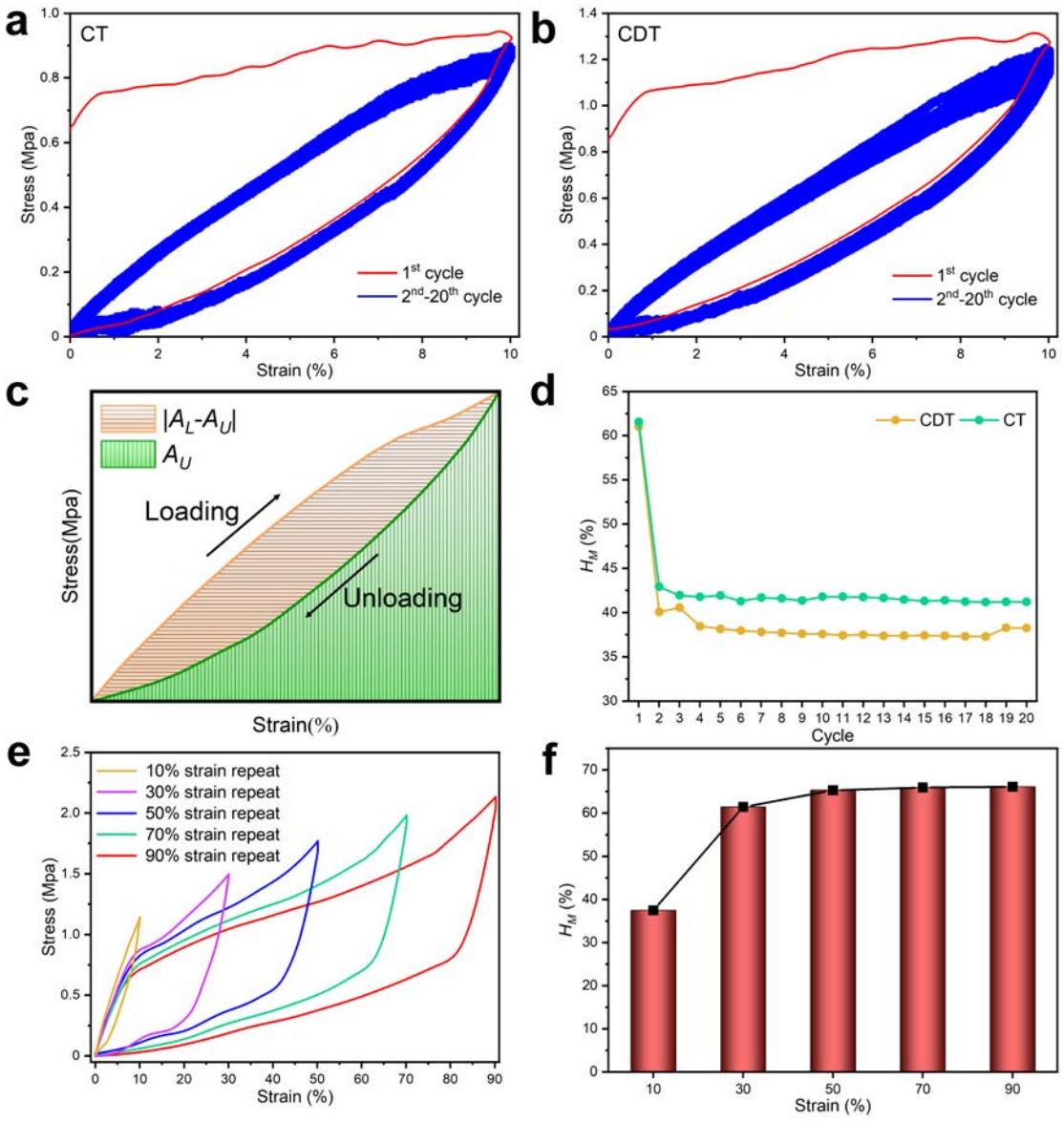

Figure. 4 a-b Cyclic stress-strain curves of CT and CDT sensors at 10% strain, c Mechanical hysteresis (H_M) quantification schematic, d H_M of CT and CDT sensors at 10% strain for 20 cycles of stretching, e Cycling stress-strain curves of CDT sensors at the strain range of 10-90%, f H_M of CDT sensors at 10-90% strain for cyclic stretching.

The H_M of the CT and CDT sensors were calculated separately for 20 cycles at 10% strain in Figure 4d. The results showed that the polydopamine-coated fibrous membrane exhibited a lower H_M. During the first cycle, the H_M was 61.53% and 60.99% for the CT and CDT, respectively, with little difference. However, during the 2-20 cycles, the average H_M of CT and CDT decreased to 41.60% and 37.97%, respectively. This is due to the plastic deformation as well as elastic deformation of TPU during the stretching - recovery process. In the first loading and unloading process, the conductive pathways of CNTs fractured for the first time, resulting in a higher tensile stress in the first loading curve. In the process of unloading, TPU fibrous membrane returned to its initial state and without any distortion, thus exhibited a relatively high H_M [68]. The sensors underwent the same process during subsequent stretching as well as recovery, but the plastic deformation of the TPU under external forces during unloading was permanent owing to the hysteresis effect of the composite and stabilized the H_M of the samples after several stretching cycles [73, 74].

The CDT sensor exhibited a lower H_M during subsequent cycles, indicating that the CDT sample to exhibit lower energy consumption as well as more excellent long-term durability than the CT sample during multiple cycles of stretching. Figures 4e and f show the twentieth cyclic stress-strain curves of CDT sensor at five strains from 10 to 90% and their corresponding H_M, respectively. The data demonstrate that the H_M of sensor at 30%, 50%, 70%, and 90% strains do not differ significantly, further demonstrating a good cyclic stability of CDT sensor.

4. Theoretical understanding of conductive fillers enabled strain sensing

Figure 5a exhibits the CNTs content as well as the polydopamine layer coated on TPU in CT as well as CDT sensors determined by thermogravimetric analysis (TGA), which can be calculated by the following equation.

$$m_{CT} = m_{CNTs1} + m_{TPU} \quad (3)$$

$$b \cdot m_{CT} = m_{CNTs1} + a \cdot m_{TPU} \quad (4)$$

$$W_{CNTs1} = \frac{m_{CNTs1}}{m_{CT}} = \frac{b-a}{1-a} \quad (5)$$

$$m_{DT} = m_{DA} + m_{TPU} \quad (6)$$

$$c \cdot m_{DT} = m_{DA} + a \cdot m_{TPU} \quad (7)$$

$$W_{DA} = \frac{m_{DA}}{m_{DT}} = \frac{c-a}{1-a} \quad (8)$$

$$m_{CDT} = m_{CNTs2} + m_{DT} \quad (9)$$

$$d \cdot m_{CDT} = m_{CNTs2} + c \cdot m_{DT} \quad (10)$$

$$W_{CNTs2} = \frac{m_{CNTs2}}{m_{CDT}} = \frac{d-c}{1-c} \quad (11)$$

Where m_{TPU}, m_{CNTs}, m_{DA} and m_{DT} are the weights of pure TPU fibrous membrane, carbon nanotubes, dopamine layer and DATPU fibrous membrane in the sensor, respectively. m_{CT} and m_{CDT} are the total weights of CT sensor and CDT sensor, respectively. For the CT sensor, the residual weight ratio of the pure TPU fibrous membrane measured after thermal degradation of the sample is *a* and the residual weight ratio of the CT sensor is *b*. Therefore, the content of CNTs in the CT sensor (W_{CNTs1}) is calculated as 15.55% according to equations (5). For the CDT sensor, the residual thermogravimetric ratio of DATPU after thermal degradation of the sample is *c*, and the residual weight ratio of the CDT sensor is *d*. Firstly, the content of dopamine (W_{DA}) coated on TPU fiber can be calculated as 0.9% according to equation (8), and then the content of CNTs in the CDT sensor (W_{CNTs2}) can be calculated by equation (11) as 17.73%. The results show that the loading of CNTs in the CDT sensor is higher than that in the CT sensor, which can further indicate that the roughness of the fiber surface can be increased due to the coating of the polydopamine layer on the TPU fibers, and more CNTs can be anchored on the fiber surface. Due to the strong interaction between the -OH in the polydopamine layer and the -COOH in the CNTs, more CNTs are anchored on the fiber surface[78-80].

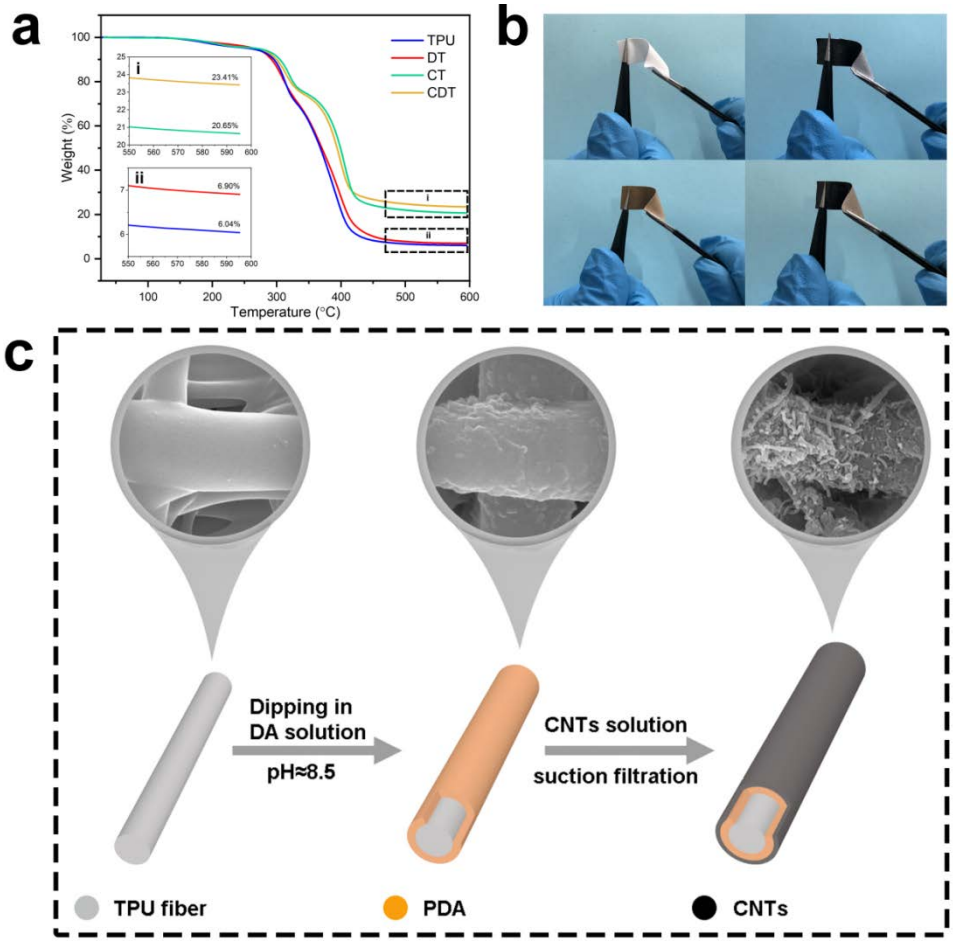

Figure. 5 a Thermogravimetric analysis of pure TPU fibrous membrane, DT fibrous membrane, CT, and CDT sensor, b Optical photos of four samples, c Demonstration of a single fiber during CDT sensor preparation.

5. Resistance fitting model for sensors

The attachment of polydopamine onto the TPU fiber surface has a significant effect on the formation of conductive network. At the microstructural level, the total resistance of CT as well as CDT sensors can be seen as a function of the *R* of every conducting filler and the resin matrix [12, 81]. The conductive fillers and conductive paths in the conductive network can be visualized as a function of the total resistance by means of a relationship curve between relative resistance and strain. The following equation is used to express the total resistance (12) [75].

$$R = \frac{M(R_m + R_c)}{N} \tag{12}$$

where R, R_m, and R_c are the total resistance of final composite, the resistance between two neighboring conductive fillers, and the resistance of single conductive filler, respectively. For electrically conductive composites, R_m is far greater than R_c, so R_m+R_c≈R_m. M is the amount of fillers building a conductive path and N is the amount of conductive paths formed. On the basis of tunneling effect theory, the resistance relationship can be expressed by the following equation [12, 82].

$$R_m = \frac{8\pi hs}{3c^2re^2} exp(rs),\ r = \frac{4\pi}{h}\sqrt{2m_e\varphi} \tag{13}$$

Substituting equation (3-13) into (3-12) gives

$$R = \frac{M}{N}\left[\frac{8\pi hs}{3c^2re^2} exp(rs)\right] \tag{14}$$

where h is Planck's constant, c^2 is the effective cross section, e is the electron charge, s is the average distance between neighboring conducting fillers, m_e is the electron mass, and φ is the height of tunnelling potential barrier.

As stress is applied to the sensor, the tunnelling distance between CNTs particles increases, and there is a process of destruction and reconstruction of the conducting path within the conducting network. Assuming that the tunnelling distance between neighbouring conducting particles satisfies a linear function from s_0 to s and the number of conducting paths satisfies an exponential function from N_0 to N, they can be calculated as follows:

$$s = s_0(1 + Ax) \tag{15}$$

$$N = N_0 exp[f(x)] \tag{16}$$

where s_0 and N_0 are the initial conductive particle distance and the initial conductive path number, respectively. x is the applied strain and $f(x)$ is a function of the strain x. A is a constant that relies on the type of conductive filler and the measurement conditions. $\Delta R/R_0$ can be obtained by substituting equation (17).

$$\frac{\Delta R}{R_0} = \frac{R-R_0}{R_0} = \frac{R}{R_0} - 1 = \left(\frac{s}{s_0} \times \frac{N_0}{N}\right) exp[r(s - s_0)] - 1$$

$$= (1 + Ax)exp[r(s - s_0) - f(x)] - 1 \tag{17}$$

where $[r(s-s_0)-f(x)]$ can be used to express the relationship between the tunneling potential height (φ) and the number of varying conducting paths (N), as Eq. (18):

$$bx^c = [r(s-s_0)-f(x)] \tag{18}$$

Substituting Eq. (18) into Eq. (17), $\Delta R/R_0$ can then be expressed as a function of strain x, as shown in equation (19).

$$\frac{\Delta R}{R_0} = (1+Ax)exp(bx^c) - 1 \tag{19}$$

where A, b, and c are constants.

For equation (16), in the actual stretching case, the conductive path of sensor will be gradually broken upon stretching, the number of conductive paths will gradually decrease with rising strain until all conductive paths break ($N \to 0$) and the sensor conductive failure, the calculation limit of which is shown below.

$$f(x) = \ln\frac{N}{N_0} \tag{20a}$$

$$\lim_{N\to 0} f(x) = \lim_{N\to 0} \ln\frac{N}{N_0} = -\infty \tag{20b}$$

Then substituting $[f(x) \to -\infty]$ into equation (16), we get:

$$bx^c = [r(s-s_0)-f(x)] \approx -f(x) \tag{21}$$

$$\frac{N}{N_0} = exp(-bx^c) \tag{22}$$

Figure 6a shows the experimental curve of $\Delta R/R_0$ depending on the strain fitted based on the model of Eq. (19). There parameters (A、b、c) calculated from the experimental test results and R^2 are showed in Table 1. The calculated data indicate that the model Eq. (19) can well verify and describe the relative resistance versus strain of CT as well as CDT sensors, and matches well with the actual test results. Figure. 6b and c show the simulated conductive path variation ratio N/N_0 and conductive interparticle distance variation ratio s/s_0 versus strain based on the parameters in Table 1 and equations (22) and (15). In Figure. 6b, according to the fitting results, it can be seen that when the strain reaches 200%, the N/N_0 of CT sample is 0.14

and the N/N_0 of CDT sample is 0.02. It could be observed that the number of conducting paths of the CDT sample is closer to 0 at 200% strain, the conductive paths in the conductive network decrease faster, which may be due to the fact that the polydopamine layer is wrapped on the TPU fiber. During the stretching, the polydopamine layer cracked and formed a special lamellar structure on the surface of TPU nanofiber, which accelerated the migration of more CNTs loaded on the polydopamine layer, leading to a faster reduction in the number of conductive paths. In Figure. 6c, the slope (s/s_0) for CDT sample is greater, the distance between the conducting particles changes faster, which well verifies the previous conjecture that the CDT sensor works as shown in Figure 6d.

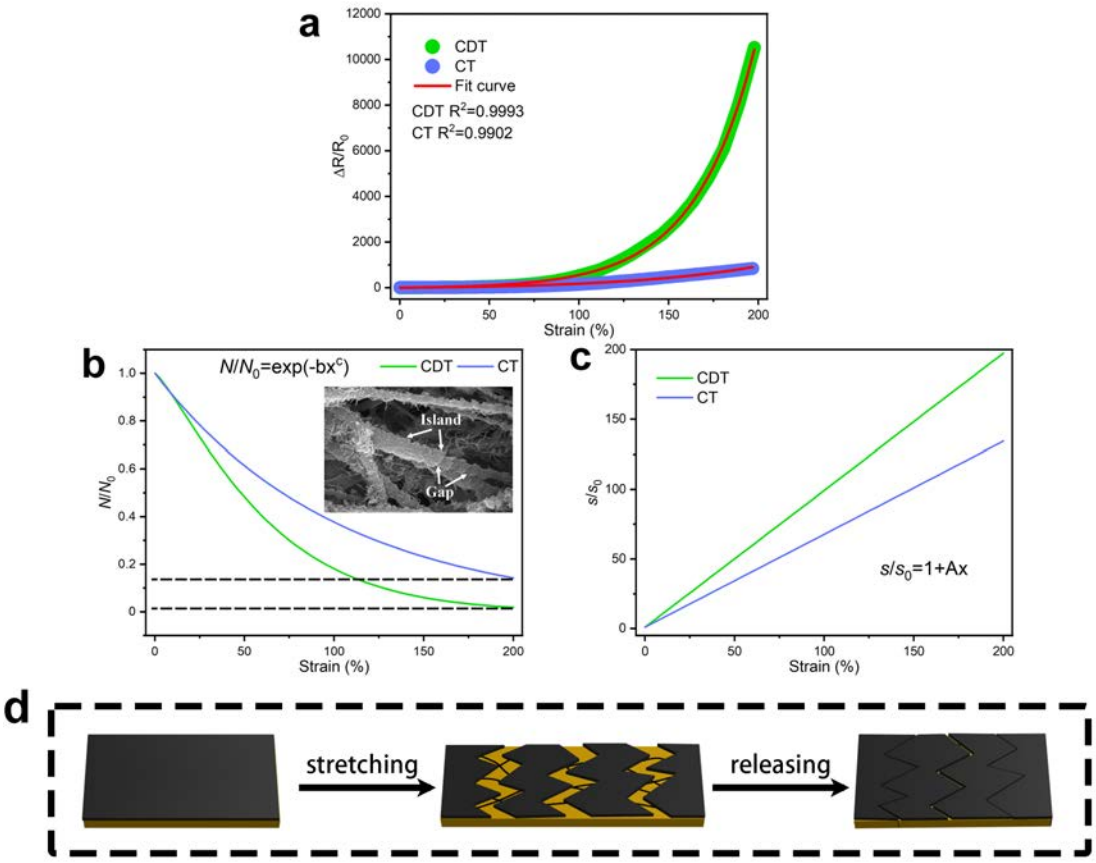

Figure. 6 a Fit function of $\Delta R/R_0$ versus strain for CT and CDT sensors and theoretical data, b Fit function of conductive path number for CT and CDT sensors, c Fit function of distance between conductive particles for CT and CDT sensors, d Schematic diagram of CDT sensor operating principle.

Table 1 Model calculation parameters of Eq. (19)

	A	b	c	R^2
CT	0.667±0.20	0.010±0.011	1.000±0.184	0.9902
CDT	0.982±0.25	0.062±0.003	1.222±0.065	0.9993

Based on the numerical model constructed by Eq. (19), the parameters (A、b、c) can visualize the level of change in the number of conductive paths and the level of change in the distance between conductive particles during the stretching process. For CT samples and CDT samples, the presence of polydopamine layers can affect the values of three parameters (Table 1). The parameter A represents the changing rate of the distance between the conducting fillers of adjacent CNTs, and the larger value of A for CDT samples compared to CT samples indicates that the distance between the conductive particles of CDT samples increases faster during stretching. The parameters b and c represent the change in conductive paths and are of great importance when analyzing the conductivity and sensitivity of the sensor. The larger values of b and c for the CDT samples compared to the CT samples indicate that the CDT samples have higher sensitivity. Normally, the interval between neighbouring conducting fillers and conducting paths is difficult to measure. Equations (15) and (22) can accurately predict the change in distance between conductive fillers and the change in the number of conductive paths during the stretching. These mathematical models have been effective in predicting the change in conductive paths and neighbouring conducting fillers.

6. Sensing performance of CDT sensors

Figure 7a and b show the repetitive electrical signal response of CDT sensor for 10 cycles at 10%, 20 and 30% strain and 50%, 70% and 100% strain, respectively, and it can be seen that the prepared CDT sample has good responsiveness. Figure 7c and d show the I-V curves of CDT sensor at microstrain (0-10%) and large strain (30-200%). The I-V curves of CDT sample

for gradual increase of voltage from -6 V to 6 V are in strict accordance with Ohm's law, which indicates the good reliability.

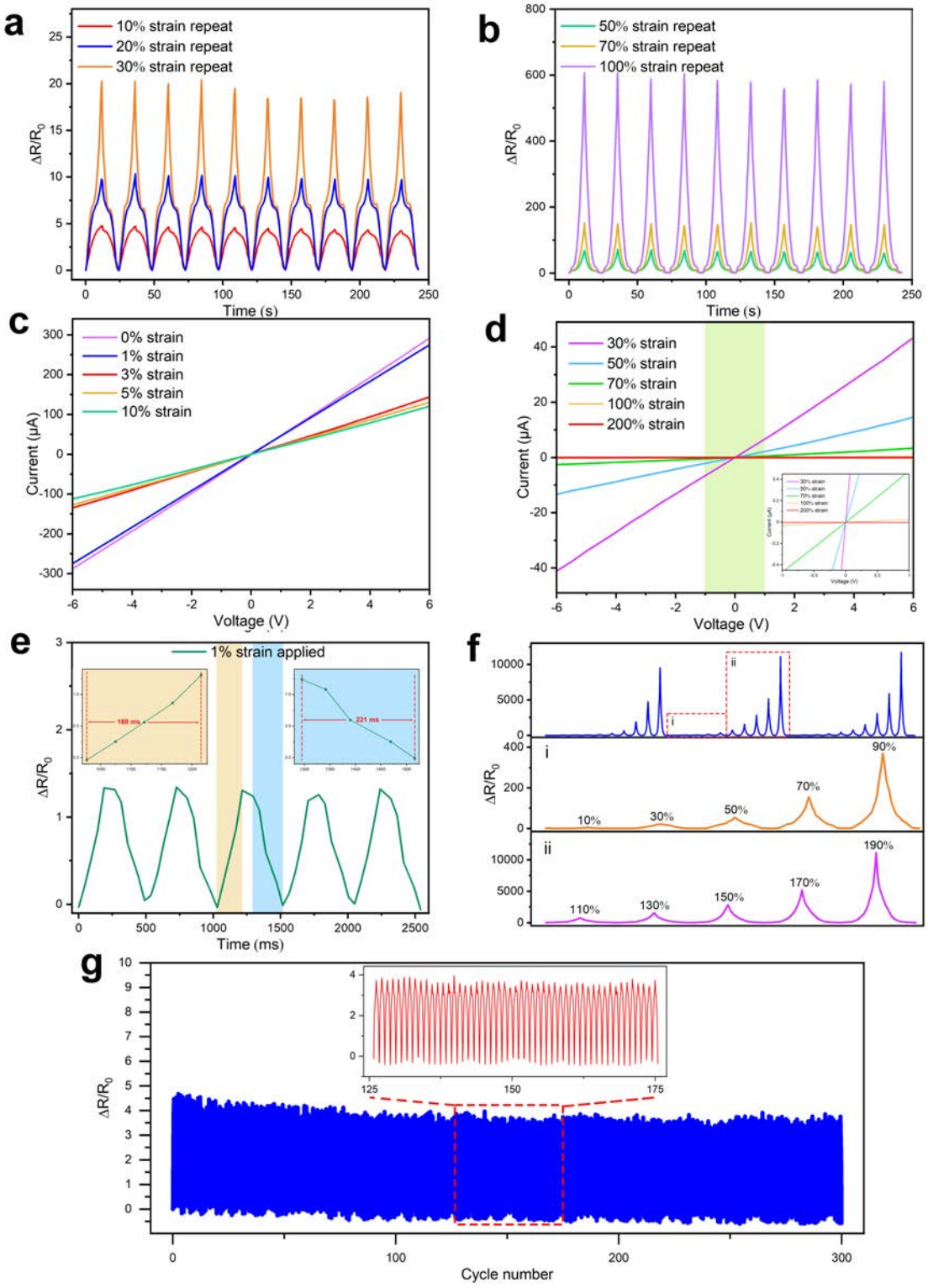

Figure 7 a-b $\Delta R/R_0$change of CDT sensor under cyclic stretching at 10-100% strain, c-d I-V curves of CDT sensor at different micro-strains and large strains, e CDT sensor response to fast

stretching, f Relative resistance change of CDT sensor at different strains for three cycles, g CDT sensor tested for 300 cycles at 10% strain at a stretching speed of 100 mm/min.

Figure 7e shows the response time measured by rapidly stretching CDT sensor at 1% strain with a stretching rate of 200 mm/min. At the loading stage, the resistance of CDT sensor rises quickly after the strain is applied, and the response time is 188 ms. At the unloading stage, the resistance of CDT sensor declines quickly after the strain is withdrawn, and the response time is 221 ms, with a difference of 33 ms. The response time increases slightly in the unloading, which may be due to the fact that the recovery of the polydopamine layer wrapped on TPU fibers at very fast stretching speed require more time, lead to the delayed re-lap of the conductive network. Figure 7f shows three cycles of testing of the CDT sample from 10% to 190% strain at each strain increase of 20%. It could be observed that the CDT sensor responds accurately to each stage of strain, further verifying that the CDT sensor has good reliability. In Figure 7g, the CDT sensor was tested for 300 cycles at 10% strain at a stretching speed of 100 mm/min, and the results showed that the CDT sensor has good stability in long-term usage.

7. Application of CDT sensors in human motion monitoring

Based on good stability and flexibility, high sensitivity and fast response capability of the CDT sensor fabricated in this work, it can be employed to monitor of the movement of human body in real-time (Figure 8a-f). As illustrated in Figure 8a and b, the resistance of CDT sensor gradually increases with the bending of finger at different bending angles (30°, 60°, and 90°) and returns to the initial position when the finger returns to its original position. In Figure 8c, when the CDT is deployed on the wrist, the CDT sensor can react to the twisting and extension of the wrist with a regular electrical signal. At the same time, the CDT sensor reacts regularly and accurately to the motions of arm and knee (Figure. 8d, e).

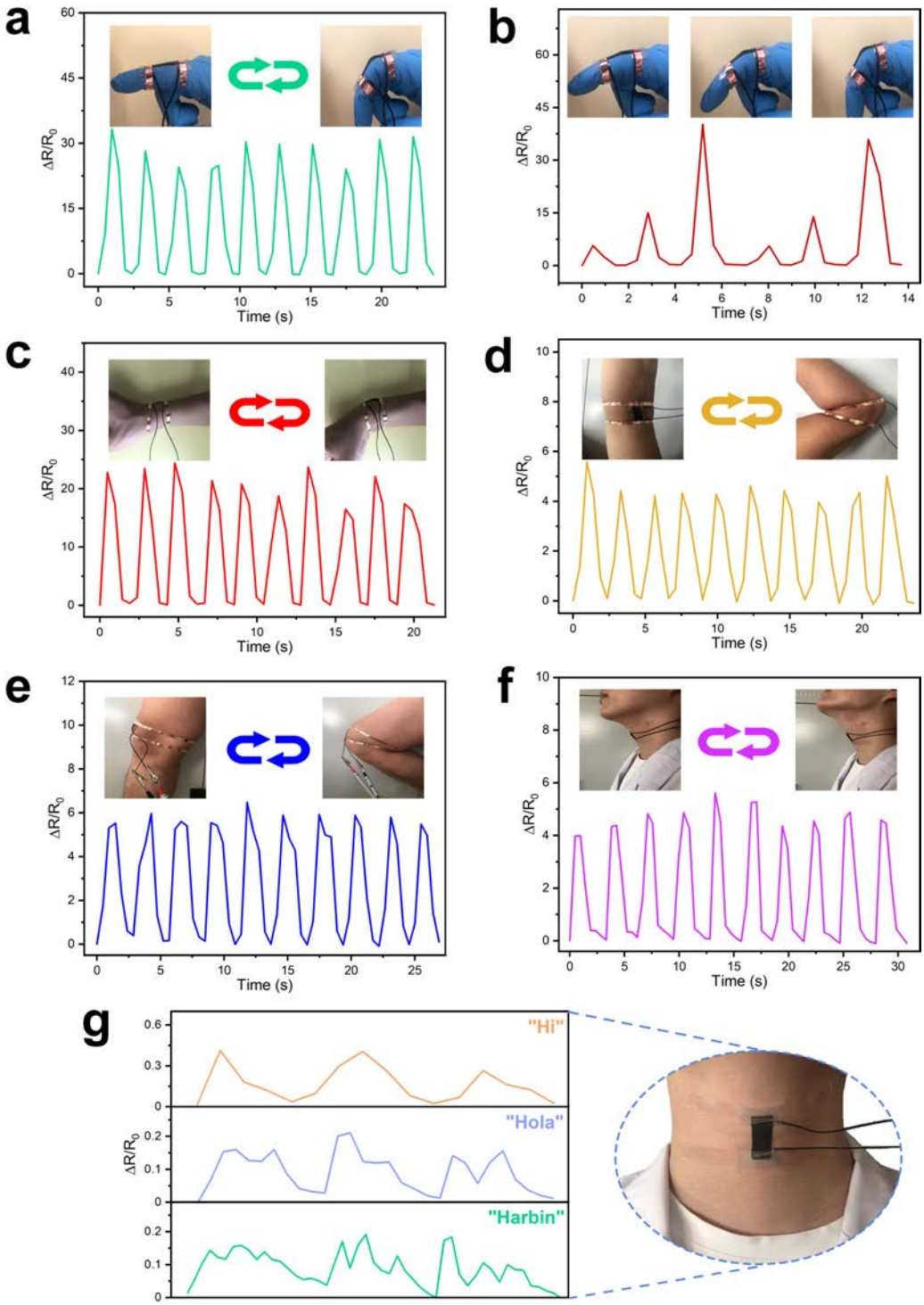

Figure 8 Sensing application of CDT strain sensors in human motion. a finger flexion, b finger flexion at 30°, 60°, 90°, c wrist flexion, d elbow flexion, e knee flexion, f head up and down, g speaking schematic.

When the CDT sensor was attached on the neck of volunteer (Figure 8f), it responds to the strain caused by raising and lowering the head. The CDT sensor could not only monitor large

human movements, but also accurately respond to the vibration of vocal folds when saying different syllables - "Hola" and "Harbin", with its excellent pressure-sensitive characteristics. By analysing the precise sensing signal including the frequency of peaks and the height of peaks in the vocal cord vibration signal, we can interpretate the number of words spoken, the frequency of speech and the volume of speech, which can be utilized to develop technology to help people with speech impairment to communicate. Therefore, the CDT sensor demonstrates significant potential in the applications such as wearable devices and human-machine interface.

4. Conclusion

The high-performance flexible strain sensors were prepared by loading CNTs on electrospun TPU fibrous membranes, and demonstrated with high sensitivity, wide detection range, good responsiveness, low price, and easy to produce on a large industrial scale. Due to the hydrogen bond interaction and strong interaction between the -OH in the polydopamine layer and the -COOH in the carbon nanotubes, more carbon nanotubes are fixed on the fiber surface, and accelerates the migration of CNTs by forming a split-layer structure when the polydopamine layer is stretched, which exhibits a faster change in resistance under stress. A mathematical model constructed by tunnel theory is used to predict the variation of conductive filler and conductive path with strain in CT and CDT samples. We find that the dopamine layer can change the fibre structure of electrospun membrane and used it to explain the origin of huge gauge factor of the flexible sensors. Owing to the high sensitivity of CDT sensors, they can be applied to the detection of small strains and various human motions.

Acknowledgments

This work was supported by Open Project Fund of the Key Laboratory of Engineering Dielectrics and Its Application (2018EDAQY05), Heilongjiang Province Postdoctoral Funded Project (LBH-Q21019), University Nursing Program for Young Scholars with Creative Talents in Heilongjiang Province (UNPYSCT-2018214), Heilongjiang Natural Science Foundation (LH2020E087), and the Engineering and Physical Sciences Research Council (EPSRC, UK) grant-EP/N007921.

Methods

Materials: TPU (Elastollan 1185A), density 1.05g/cm^3, was provided by BASF Co., Ltd. Carbon nanotubes (MWCNT-COOH, diameter from 20 to 40 nm, length less than 5 microns) were purchased from Shenzhen Nanotech Port Co., Ltd. N, N-dimethylformamide (DMF) and tetrahydrofuran (THF) were purchased from Tianjin Fuyu Fine Chemical Co., Ltd. Dopamine hydrochloride (DA·HCl) and Sodium periodate ($NaIO_4$) were purchased from Shanghai Macklin Biochemical Co., Ltd. Tris (hydroxymethyl) aminomethane (Tris) was purchased from Fuzhou Feijing Biological Technology Co., Ltd.

Preparation of TPU fibrous membrane through electrospinning: TPU fibrous membrane were prepared using electrostatic spinning technique. Firstly, TPU particles with a mass fraction of 20% were dissolved in a mixture of DMF/THF (mass ratio of 1:1). The mixture was mechanically stirred at room temperature for 5 h to obtain a homogeneous spinning solution. Then, the spinning solution was injected into a syringe with a capacity of 15 ml for electrostatic spinning. Aluminum foil was chosen to be laid on the roller as the receiving device for TPU fibers, the receiving distance between the needle and receiving rollers was 20 cm, and electrostatic spinning was carried out at 20 kV and the liquid supply rate was 1 ml/h. Lastly, the prepared fiber films were dried at 85 °C for 5 h to eliminate the residual organic solvent.

Preparation of dopamine-coated TPU fibrous membrane: First, the TPU fibrous membrane was repeatedly washed with purified water to eliminate surface pollutant and then dried in an oven at 65°C for 3 h. The TPU nanofibers mats was coated and finely modified using the fast polydopamine coating method (fPDAc) [83, 84], specifically an aqueous solution of DA/tris (10 mM, pH 8.5) at 2.0 g/L and DA with $NaIO_4$ (10 mM, pH 8.5) with a molar ratio of 0.5 was immediately mixed, and the TPU electrospun membrane was immersed in it and stirred continuously, and the surface of the TPU electrospun membrane changed from light pink to brown with the spontaneous deposition of the attached polydopamine (PDA) layer. Finally, the PDA-coated TPU fibrous membrane was rinsed with purified water for 30 min and dried in an oven at 65°C for 3 h to produce the DATPU fibrous membrane.

Preparation of CNTs/TPU and CNTs/DATPU strain sensors: Firstly, 2.0 g/L of CNTs aqueous solution was sonicated for 2 h to produce a uniformly dispersed CNTs suspension. Then, the TPU electrospun membrane and DATPU film were cut into 50 mm × 50 mm size and the CNTs suspension was filtered onto the TPU electrospun membrane and DATPU film with 2.5 ml, 5 ml, 7.5 ml, 10.5 ml, 15 ml and a certain amount and rinsed 3 times with purified water and dried at 80°C. Finally, filtered CNTs of TPU electrospun membrane and DATPU film were cut into 10 mm × 40 mm segments and connected to wires for the convenience of testing as CT and CDT flexible strain sensors.

Characterization: Scanning electron microscopy (SEM, Volumescope2, Thermo Scientific, America) was employed to observe the morphology of the samples at an accelerating voltage of 5 kV.

Tensile tests were performed with an electronic universal testing apparatus (UTM2203, SUN, China) equipped with a 2 kN transducer at a rate of 50 mm/min. All specimens are in size of 40 mm × 10 mm with an applied length of 20 mm. 5 tests were performed on all specimens and the average value was taken.

To acquire the I-V curves of the sensors, static resistance measurements were performed with a digital source meter (Keithley 2400, USA) at an applied voltage(- 6 to + 6 V) .

The sensing performance was characterized with the digital source meter (Keithley 2400) in conjunction with a UTM2203 electronic universal testing machine. A sensor sample of size 40 mm × 10 mm was first fixed on the universal mechanical testing machine at a distance of 20 mm from both ends of the fixture, after which the digital source meter was connected to either ends of the sensor and used to test the resistance versus strain of the CT and CDT sensors at a constant tensile rate of 10 mm/min. The relative resistance change can be calculated by Eq. 23.

$$\Delta R/R_0 = (R - R_0)/R_0 \quad (23)$$

Where R_0 is the initial resistance when ε=0% and R is the real time resistance varies with strain.

References

[1] N. Wen, L. Zhang, D. Jiang, Z. Wu, B. Li, C. Sun, Z. Guo, J. Mater. Chem. A **2020**, 8(48), 25499-25527.
[2] M. Fan, L. Wu, Y. Hu, M. Qu, S. Yang, P. Tang, L. Pan, H. Wang, Y. Bin, Adv. Compos. Hybrid Mater **2021**, 4, 1039–1047.
[3] D. Zhang, M. Zhang, J. Wang, H. Sun, H. Liu, L. Mi, C. Liu, C. Shen, Adv. Compos. Hybrid Mater **2022**, 5, 1812–1820.
[4] M. Hu, Y. Gao, Y. Jiang, H. Zeng, S. Zeng, M. Zhu, G. Xu, L. Sun, Adv. Compos. Hybrid Mater **2021**, 4, 514–520.
[5] X. Chang, L. Chen, J. Chen, Y. Zhu, Z. Guo, Adv. Compos. Hybrid Mater **2021**, 4, 435–450.
[6] Y. Shen, W. Yang, F. Hu, X. Zhang, Y. Zheng, H. Liu, H. Algadi. K. Chen, Adv. Compos. Hybrid Mater **2023**, 6, 21.
[7] X. Liu, Z. Wu, D. Jiang, Adv. Compos. Hybrid Mater **2022**, 5(3):1712-1729.
[8] J. C. Yang, J. Mun, S. Y. Kwon, S. Park, Z. Bao, S. Park, Adv Mater **2019**, 31, e1904765.
[9] D. J. Lipomi, M. Vosgueritchian, B. C. Tee, S. L. Hellstrom, J. A. Lee, C. H. Fox, Z. Bao, Nat Nanotechnol **2011**, 6, 788.
[10] X. Yue, Y. Jia, X. Wang, K. Zhou, W. Zhai, G. Zheng, K. Dai, L. Mi, C. Liu, C. Shen, Compos. Sci. Technol **2020**, 189.
[11] S. Wang, Y. Fang, H. He, L. Zhang, C. a. Li, J. Ouyang, Adv. Funct. Mater **2020**, 31.
[12] J. Huang, D. Li, M. Zhao, A. Mensah, P. Lv, X. Tian, F. Huang, H. Ke, Q. Wei, Adv. Electron. Mater **2019**, 5.
[13] M. Amit, L. Chukoskie, A. J. Skalsky, H. Garudadri, T. N. Ng, Adv. Funct. Mater **2019**, 30.
[14] T. Q. Trung, N. E. Lee, Adv Mater **2016**, 28, 4338.
[15] Z. Lou, L. Wang, K. Jiang, Z. Wei, G. Shen, Mater. Sci. Eng., R **2020,** 140.
[16] S. Choi, S. I. Han, D. Jung, H. J. Hwang, C. Lim, S. Bae, O. K. Park, C. M. Tschabrunn, M. Lee, S. Y. Bae, J. W. Yu, J. H. Ryu, S. W. Lee, K. Park, P. M. Kang, W. B. Lee, R. Nezafat, T. Hyeon, D. H. Kim, Nat Nanotechnol **2018**, 13, 1048.
[17] H. Lee, T. K. Choi, Y. B. Lee, H. R. Cho, R. Ghaffari, L. Wang, H. J. Choi, T. D. Chung, N. Lu, T. Hyeon, S. H. Choi, D. H. Kim, Nat Nanotechnol **2016**, 11, 566.
[18] H. Joo, Y. Lee, J. Kim, J. S. Yoo, S. Yoo, S. Kim, A. K. Arya, S. Kim, S. H. Choi, N. Lu, H. S. Lee, S. Kim, S. T. Lee, D. H. Kim, Sci Adv **2021**, 7.
[19] K. Xu, Y. Fujita, Y. Lu, S. Honda, M. Shiomi, T. Arie, S. Akita, K. Takei, Adv Mater **2021**, 33, e2008701.
[20] S. C. Mannsfeld, B. C. Tee, R. M. Stoltenberg, C. V. Chen, S. Barman, B. V. Muir, A. N. Sokolov, C. Reese, Z. Bao, Nat Mater **2010**, 9, 859.
[21] D. Wang, Y. Lin, D. Hu, P. Jiang, X. Huang, Composites Part A **2020**, 130.
[22] Z. Chu, W. Jiao, Y. Huang, Y. Zheng, R. Wang, X. He, J. Mater. Chem. A **2021**, 9, 9634.
[23] X. Zhou, L. Zhu, L. Fan, H. Deng, Q. Fu, ACS Appl. Mater. Interfaces **2018**, 10, 31655.
[24] Z. H. Yang, Z. J. Wu, D. W. Jiang, J. Mater. Chem. C **2021**.
[25] H. Liu, J. Gao, W. Huang, K. Dai, G. Zheng, C. Liu, C. Shen, X. Yan, J. Guo, Z. Guo, Nanoscale **2016**, 8, 12977.
[26] L. Lin, Y. Choi, T. Chen, H. Kim, K. S. Lee, J. Kang, L. Lyu, J. Gao, Y. Piao, Chem. Eng. J **2021**, 419.
[27] K. Ke, V. Solouki Bonab, D. Yuan, I. Manas-Zloczower, Carbon **2018**, 139, 52.
[28] M. Amjadi, Y. J. Yoon, I. Park, Nanotechnology **2015**, 26, 375501.
[29] M. Xu, J. Qi, F. Li, Y. Zhang, Nanoscale **2018**, 10, 5264.
[30] L. Lu, X. Wei, Y. Zhang, G. Zheng, K. Dai, C. Liu, C. Shen, J. Mater. Chem. C **2017**, 5, 7035.
[31] F. Guan, Y. Xie, H. Wu, Y. Meng, Y. Shi, M. Gao, Z. Zhang, S. Chen, Y. Chen, H. Wang, Q. Pei, ACS Nano **2020**, 14, 15428.
[32] G. J. Zhu, P. G. Ren, J. Wang, Q. Duan, F. Ren, W. M. Xia, D. X. Yan, ACS Appl. Mater. Interfaces **2020**, 12, 19988.
[33] S. Zhang, H. Liu, S. Yang, X. Shi, D. Zhang, C. Shan, L. Mi, C. Liu, C. Shen, Z. Guo, ACS Appl. Mater. Interfaces **2019**, 11, 10922.
[34] R. Yin, S. Yang, Q. Li, S. Zhang, H. Liu, J. Han, C. Liu, C. Shen, Sci. Bull. **2020**, 65, 899.
[35] D. Jiang, Y. Wang, B. Li, C. Sun, Z. Wu, H. Yan, L. Xing, S. Qi, Y. Li, H. Liu, W. Xie, X. Wang, T. Ding, Z. Guo, Polym. Rev **2019**, 304 (7), 1900074.
[36] Y. Zhou, P. Zhan, M. Ren, G. Zheng, K. Dai, L. Mi, C. Liu, C. Shen, ACS Appl. Mater. Interfaces **2019**, 11, 7405.
[37] Z. Niu, W. Yuan, ACS Appl. Mater. Interfaces **2021**, 13, 4508.
[38] M. Qu, H. Wang, Q. Chen, L. Wu, P. Tang, M. Fan, Y. Guo, H. Fan, Y. Bin, Chem. Eng. J **2022**, 427.
[39] J. S. Heo, R. Soleymanpour, J. Lam, D. Goldberg, E. Large, S. K. Park, I. Kim, IEEE J. Biomed Health Inform **2022**, 26, 581.

[40] Y. Fei, F. Chen, W. Fang, A. Hejna, L. Xu, T. Liu, M. Zhong, J. Yang, T. Kuang, J. Mater. Chem. C **2021**, 9, 13103.
[41] B. Li, J. Luo, X. Huang, L. Lin, L. Wang, M. Hu, L. Tang, H. Xue, J. Gao, Y.-W. Mai, Composites Part B **2020**, 181.
[42] Q. Zheng, J.-h. Lee, X. Shen, X. Chen, J.-K. Kim, Mater. Today **2020**, 36, 158.
[43] Y. Li, T. He, L. Shi, R. Wang, J. Sun, ACS Appl. Mater. Interfaces **2020**, 12, 17691.
[44] L. Q. Tao, K. N. Zhang, H. Tian, Y. Liu, D. Y. Wang, Y. Q. Chen, Y. Yang, T. L. Ren, ACS Nano **2017**, 11, 8790.
[45] M. Qu, F. Nilsson, Y. Qin, G. Yang, Y. Pan, X. Liu, G. Hernandez Rodriguez, J. Chen, C. Zhang, D. W. Schubert, Compos. Sci. Technol. **2017**, 150, 24.
[46] L. V. Kayser, D. J. Lipomi, Adv Mater **2019**, 31, e1806133.
[47] X. Wang, J. Zhou, Y. Zhu, W. Cheng, D. Zhao, G. Xu, H. Yu, Chem. Eng. J **2020**, 392.
[48] E. Roh, B. U. Hwang, D. Kim, B. Y. Kim, N. E. Lee, ACS Nano **2015**, 9, 6252.
[49] G. Ge, Y. Cai, Q. Dong, Y. Zhang, J. Shao, W. Huang, X. Dong, Nanoscale **2018**, 10, 10033.
[50] Y. Zheng, R. Yin, Y. Zhao, H. Liu, D. Zhang, X. Shi, B. Zhang, C. Liu, C. Shen, Chem. Eng. J **2021**, 420.
[51] W. Chen, L. X. Liu, H. B. Zhang, Z. Z. Yu, ACS Nano **2021**, 15, 7668.
[52] X. Zheng, J. Shen, Q. Hu, W. Nie, Z. Wang, L. Zou, C. Li, Nanoscale **2021**, 13, 1832.
[53] N. Bhardwaj, S. C. Kundu, Biotechnol. Adv. **2010**, 28, 325.
[54] H. Yoshimoto, Y. M. Shin, H. Terai, J. P. Vacanti, Biomater **2003**, 24, 2077.
[55] Y. Qin, D. W. Schubert, Polym **2019**, 181.
[56] H. Ziyadi, M. Baghali, M. Bagherianfar, F. Mehrali, R. Faridi-Majidi, Adv. Compos. Hybrid Mater **2021**, 4, 768–779.
[57] Z. Zhang, Y. Zhao, Z. Li, L. Zhang, Z. Liu, Z. Long, Y. Li, Y. Liu, R. Fan, K. Sun, Z. Zhang, Y. Qin, D. W. Schubert, Polym **2019**, 181.
[58] M. Ren, Y. Zhou, Y. Wang, G. Zheng, K. Dai, C. Liu, C. Shen, Chem. Eng. J **2019**, 360, 762.
[59] Y. X. Song, W. M. Xu, M. Z. Rong, M. Q. Zhang, Adv. Compos. Hybrid Mater **2022**, 5, 513–524.
[60] R. Liu, J. G. Kim, P. Dhakal, W. Li, J. Ma, A. Hou, C. Merkel, J. Qiu, M. Zoran, S. Wang, Adv. Compos. Hybrid Mater **2019**, 6, 14.
[61] S. Sharafkhani, M. Kokabi, Adv. Compos. Hybrid Mater **2022**, 5, 3081–3093.
[62] M. Liu, H. Wu, Y. Wu, P. Xie, R. A. Pashameah, H. M. Abo-Dief, S. M. EI-Bahy, Y. Wei, G. Li, W. Li, G. Liang, C. Liu, K. Sun, R. Fan, Adv. Compos. Hybrid Mater **2022**, 5, 2021–2030.
[63] P. Wang, T, Song, H, M. Abo-Dief, J. Song, A. K. Alanazi, B. Fan, M. Huang, Z. Lin, A. A. Altalhi, S. Gao, L. Yang, J. Liu, S. Feng, T. Cao, Adv. Compos. Hybrid Mater **2022**, 5, 1100–1110.
[64] Z. Yan, S. Wang, J. Bi, Q. He, H. Song, I. H. E. Azab, S. M. EI-Bahy, A. Y. Elnaggar, M. Huang, M. H. H. Mahmoud, J. Wang, Q. Shao, Adv. Compos. Hybrid Mater **2019**, 5, 2116–2130.
[65] L. Song, J. Chen, B. B. Xu, Y. Huang, ACS Nano **2021**, 15, 12.
[66] B. B. Xu, Q. Liu, Z. Suo, R. C. Hayward, Adv. Funct. Mater **2016**, 26, 3218.
[67] H. Wei, Z. Wang, H. Zhang, Y. Huang, Z. Wang, Y. Zhou, B. B. Xu, S. Halila, J. Chen, Chem. Mater **2021**, 33, 17.
[68] X. Dai, Y. Du, Y. Wang, Y. Liu, N. Xu, Y. Li, D. Shan, B. B. Xu, J. Kong, ACS Appl. Polym. Mater **2020**, 2, 3.
[69] Z. Wang, H. Zhou, D. Liu, X. Chen, D. Wang, S. Dai, F. Chen, B. B. Xu, Adv. Funct. Mater **2022**, 32.
[70] Y. Liu, A. Sun, S. Sridhar, Z. Li, Z. Qin, J. Liu, X. Chen, H. Lu, B. Z. Tang, B. B. Xu, ACS Appl. Mater. Interfaces **2021**, 13, 30.
[71] Z. Li, Y. Liu, M. Lei, A. Sun, S. Sridhar, Y. Li, X. Liu, H. Lu, Y. Q. Fu, B. B. Xu, Soft Matter **2020**, 16, 1636.
[72] H. Li, J. Chen, X. Chang, Y. Xu, G. Zhao, Y. Zhu, Y. Li, J. Mater. Chem. A **2021**, 9, 1795.
[73] C. Lozano-Pérez, J. V. Cauich-Rodríguez, F. Avilés, Compos. Sci. Technol. **2016**, 128, 25.
[74] Y. Wang, Y. Jia, Y. Zhou, Y. Wang, G. Zheng, K. Dai, C. Liu, C. Shen, J. Mater. Chem. C **2018**, 6, 8160.
[75] X. Wang, X. Liu, D. W. Schubert, Nanomicro Lett **2021**, 13, 64.
[76] J. Lin, W. Wang, J. Cheng, Z. Cui, J. Si, Q. Wang, W. Chen, J. Appl. Polym. Sci. **2020**, 137.
[77] Y. Li, B. Zhou, G. Zheng, X. Liu, T. Li, C. Yan, C. Cheng, K. Dai, C. Liu, C. Shen, Z. Guo, J. Mater. Chem. C **2018**, 6, 2258.
[78] J. F. Guan, J. Zou, P. Y. Liu, Y. X. Jiang, G. J. Yu, Ecotoxicol. Environ. Saf. **2020, 201, 110872.**
[79] H. Bi, Y. Li, S. Liu, P. Guo, Z. Wei, C. Lv, Sens. Actuators **2018**, 171, 1132.
[80] G. Xu, B. Li, T. X. Cui, L. Ling, X. Luo, Sens. Actuators, B **2018**, 188, 405.
[81] X.-W. Zhang, Y. Pan, Q. Zheng, X.-S. Yi, J. Polym. Sci., Part B: Polym. Phys **2000**, 38, 2739.
[82] S. Zhao, D. Lou, G. Li, Y. Zheng, G. Zheng, K. Dai, C. Liu, Y. Jiang, C. Shen, Compos. Sci. Technol. **2018**, 163, 18.
[83] S. H. Hong, S. Hong, M.-H. Ryou, J. W. Choi, S. M. Kang, H. Lee, Adv. Mater. Interfaces **2016**, 3.
[84] J. Wang, H. Guo, X. Shi, Z. Yao, W. Qing, F. Liu, C. Y. Tang, J. Colloid Interface Sci. **2019**, 535, 239.